SPACE RESEARCH
REVIEW

VOLUME 2
2013

ENGINEERING RESEARCH INSTITUTE
VENTSPILS INTERNATIONAL RADIO ASTRONOMY CENTRE
OF THE VENTSPILS UNIVERSITY COLLEGE

VENTSPILS

Space Research Review

Established in 2012 by the Engineering Research Institute „Ventspils International Radio Astronomy Centre" of Ventspils University College.

Aims and Scope

Space Research Review is once per two years published peer-reviewed international Journal intended for publication of broad-spectrum original articles, reviews and short communications in actual problems of frontier space technologies: space science, including space and atmospheric physics, Earth observation and remote sensing from space, planetary sciences, astrochemistry, astrobiology and life sciences, and space-based astronomy and astrophysics; space engineering, including communications, navigation, space operations, satellite design, testing, and implementation, engineering, modernisation and design of new generation telescopes; space IT solutions, including data acquisition, signal processing, data correlation, parallel and high performance and cloud computing techniques; as well as innovations in space education and training.

© Copyright

Space Research Review Online

Space Research Review is available online at http://www.virac.eu

Acknoweledgement to Referees

The Editors of Space Research Review would like to thank the many scientists who contributed so generously of their time and expertise to referee papers submitted to the Journal.

Abstracted and indexed

Attention! The databases (like Springer, EBSCO, VINITI, Google Scholar etc.) select the papers from this edition for including them in their data bases after individual qualitative examination.

Subscription information

Engineering Research Institute „Ventspils International Radio Astronomy Centre" of Ventspils University College, Inzenieru 101, LV 3600, Ventspils, Latvia.
E-mail: virac@virac.lv

Journal Policy

Engineering Research Institute „Ventspils International Radio Astronomy Centre" of Ventspils University College assumes no responsibility for views, statements and opinions expressed by contributors. Any reference to content, prototype or other commercial or proprietary product does not constitute a recommendation or an endorsement of its use by the author(s), their institution or any person connected with preparation, publication or distribution of this Journal.

ISBN 978-9984-648-33-0

2nd International Scientific Conference of
Ventspils International Radio Astronomy Centre
15 – 16 May, 2013, Ventspils, Latvia

Baltic Applied Astroinformatics and Space Data Processing

BAASP2013

Dear reader!

Engineering Research Institute „Ventspils International Radio Astronomy Centre" of the Ventspils University College in cooperation with our partners in Ventspils, Baltic States and worldwide proudly present selected papers from the 2nd Baltic Applied Astroinformatics and Space Data Processing Conference: BAASP2013.

Representatives from more than 10 countries provided 26 reports with a focus to the astronomy, astrophysics, space technologies and informatics aspects related to interdisciplinary research in astroinformatics and space data engineering. The scope of the conference covered atmospheric physics, Earth observation and remote sensing, astrochemistry, space communications, navigation, satellite design, testing, and implementation, engineering of new generation telescopes, as well as space data acquisition, buffering, signal processing, data correlation, data recording, transfer, processing and archiving, high performance and cloud computing techniques.

During the next decade, astronomy is facing a major data avalanche: the next-generation astronomy data digital archives will cover most of the sky at fine resolution in many wavelengths, from X-rays, through ultraviolet, optical, and infrared. The observational astronomy is rapidly changing its nature as large digital sky surveys are becoming the dominant source of data ordering of magnitude larger, more complex, more homogeneous and more complete physical picture; the resulting complexity of data translates into increased demands for data analysis, visualization, and understanding.

We are confident that Conference BAASP2013 has continued new research tradition in Ventspils city demonstrating high scientific level, providing meeting platform and generating fruitful discussions on global and regional science and technology scene.

Valdis Avotiņš,
Director of VIRAC

Scientific Organising Committee members

Dr. Dmitrijs Docenko (chairman) – University of Latvia,

Institute of Astronomy (Latvia);

Dr. Arunas Andziulis – University of Klaipeda (Lithuania);

Dr. Guntars Balodis – Riga Technical University (Latvia);

Dr. Rihards Balodis – University of Latvia,

Institute of Mathematics and Computer Science (Latvia);

Dr. Juris Borzovs – University of Latvia (Latvia);

Dr. Dainis Dravins – Lund Observatory (Sweden);

Dr. Ilgmars Eglitis – University of Latvia, Institute of Astronomy (Latvia);

Dr. Juris Freimanis – Ventspils University College (Latvia);

Dr. Janis Grundspenkis - Riga Technical University (Latvia);

Dr. Normunds Jekabsons – Ventspils University College (Latvia);

Dr. Algimantas Juozapavicius – Vilnius University (Lithuania);

Dr. Janis Kaminskis – Riga Technical University (Latvia);

Dr. Mart Noorma – University of Tartu (Estonia);

Dr. Anu Reinart – Tartu Observatory (Estonia);

Dr. Boriss Rjabovs – Ventspils University College (Latvia) ;

Dr. Danguole Rutkauskiene – Kaunas University of Technology (Lithuania);

Dr. Ivars Smelds – Ventspils University College (Latvia);

Dr. Grazina Tautvaisiene – Vilnius University (Lithuania);

Dr. Andris Vaivads – Swedish Institute of Space Physics (Sweden);

Dr. Laimons Zacs – Laser Centre of University of Latvia (Latvia);

Dr. Hab. Juris Zagars – Ventspils University College (Latvia).

Local Organizing Committee

Dr. Valdis Avotins (chairman)

Santa Kalvane

Liene Riekstina

Livija Aulmane

Ieva Kozlova

Egils Vitols

Content

MICROWAVE OBSERVATIONS OF THE SUN WITH THE RT-32 SPECTROPOLARIMETER: PROGRESS REPORT

D. A. Bezrukov, B. I. Ryabov

Engineering Research Institute "Ventspils International Radio Astronomy Center" of Ventspils University College, Inzenieru str., 101, Ventspils, LV-3601, Latvia

Abstract. The goal of the observations by the multichannel spectral polarimeter with the RT-32 radio telescope of the Ventspils International Radio Astronomy Center is the set of 16 brightness temperature maps of the solar emission within the 3.2 - 4.7 cm wavelength range. These solar observations mapping, calibration and deconvolution methods are discussed.

Key words: Sun, solar radio astronomy

1. Introduction

The new 16-channel solar spectral polarimeter were implemented and tested on the basis of the RT-32 radio telescope of the Ventspils International Radio Astronomy Center (VIRAC) (Bezrukov 2013). The spectral polarimeter provides both the R and L circular polarization observations of the solar microwave emission in the 3.2 - 4.7 cm wavelength band. The observations of the Sun by the spectral polarimeter are covering the lack of information about the solar emission at this wavelength band and aimed to effective solutions of the relevant solar physics problems.

The result of the automated observations by RT-32 radio telescope and the data processing is expected in the form of Stokes I and V maps of the Sun available at 16 wavelengths. The mapping, calibration and deconvolution procedures and software for these observations were developed.

2. Mapping

Observations of the whole Sun were performed by the azimuthal scanning. During the observation the antenna moves along the azimuth at a constant angular speed shifting vertically by a half of the antenna pattern HPBW at the shortest wavelength (1.2 arcmin) in relation to the geometrical center of the Sun. The full scanning of the Sun takes about 1.5 hours and yields 28÷30 scan. The observation result is 32 sets of the 1D antenna temperature scans (Fig. 1). The sampling frequency of the spectral polarimeter is about 80 Hz and each scan consists of about 1500-1800 samples.

The 2D map of radio brightness generated from the 1D antenna temperature scan set includes the horizontal antenna coordinates recalculation to their local coordinates onto the screen plane in relation to the current center of the Sun for each sample. Next, the recalculated sample set is converted to the regular 2D grid using the bilinear interpolations of the absent pixels. Finally the both circular R and L polarization maps are converted to Stokes I and V maps (Fig.2).

3. Precision of the measurements

In the case of the solar observations with the RT-32 radio telescope the origin of mistakes of the real solar brightness temperature distribution is

- the errors of the antenna temperature measurements
- the errors of the antenna horizontal coordinate measurements,
- the finite size and irregularities of the radio telescope antenna pattern.

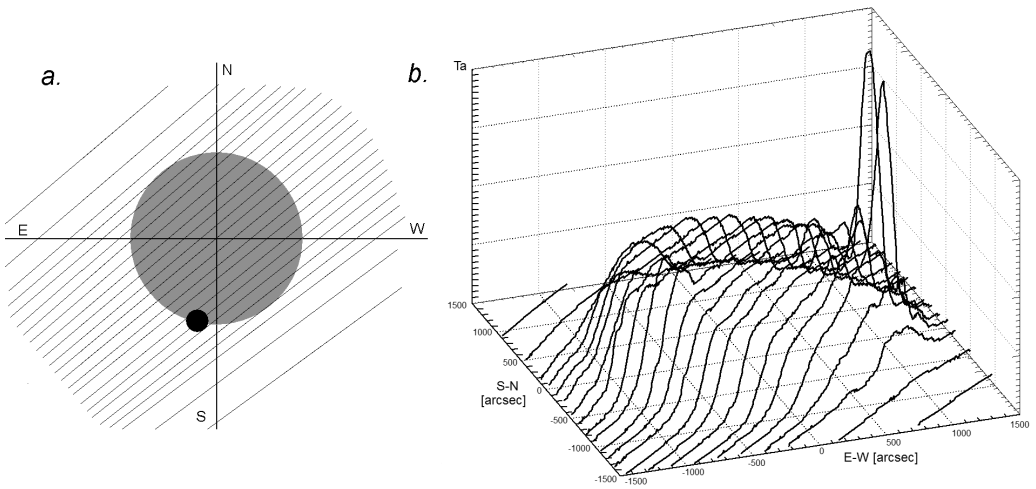

Fig. 1. *The tracks of the Sun's azimutal scanning telescope on 2012, July 17 UT 7:15 in relation to the center of the Sun and the Sun's axes. The black spot presents the antenna HPBW(a) at the 3.76 cm wavelength. The set of 1D scans of the antenna temperature (b)*

The measured system noises and cross polarization interferences differ from channel to channel but do not exceed 20 dB at the hardware time constant about 10 msec (Bezrukov 2013). It means that the relative antenna temperature measurement precision is about 1 - 1.5 %. Increasing the measurement time constant to 1 sec it is possible to increase the antenna temperature measurement precision to 10 dB (the relative measurement precision about 0.1 - 0.15%).

The determination precision of the position of electrical antenna axis is limited by the antenna angle sensor's discretization (1 bit = 20 arcsec), the systematic electrical antenna axis displacement from the geometrical and the systematic geometrical antenna axis displacement from the real local horizontal coordinates. Thus, the error of the antenna position measurement is ±10 arcsec for each axis. The antenna angle sensor systematic errors and the antenna pattern of the radio telescope RT-32 have been studied sufficiently by the regular calibration source observations (Bezrukovs & Ozolinsh 2012). The electrical antenna axis displacement from the local horizontal coordinates is about 1.5 - 2 arcmin for each axis and depends on the antenna elevation. The RT-32 antenna pointing system automatically compensates these errors until the angle sensors discretization value. Taking into account the Gaussian approximation of the antenna pattern the relative precision of the antenna temperature caused by the antenna position errors is about 1.5% at the shortest wavelength.

4. Calibration

The spectral polarimeter is meant for the antenna temperature measurements. As the spectral polarimeter is not sensitive enough to detect faint point-like microwave sources we make use of the Sun itself as the calibration source. To express the observed antenna temperature maps in units of the brightness temperature we adopt the permanent values of the known quiet Sun brightness temperature for each map. The quiet Sun brightness temperatures (Borovik et al. 1992) are linearly interpolated for the corresponding wavelengths.

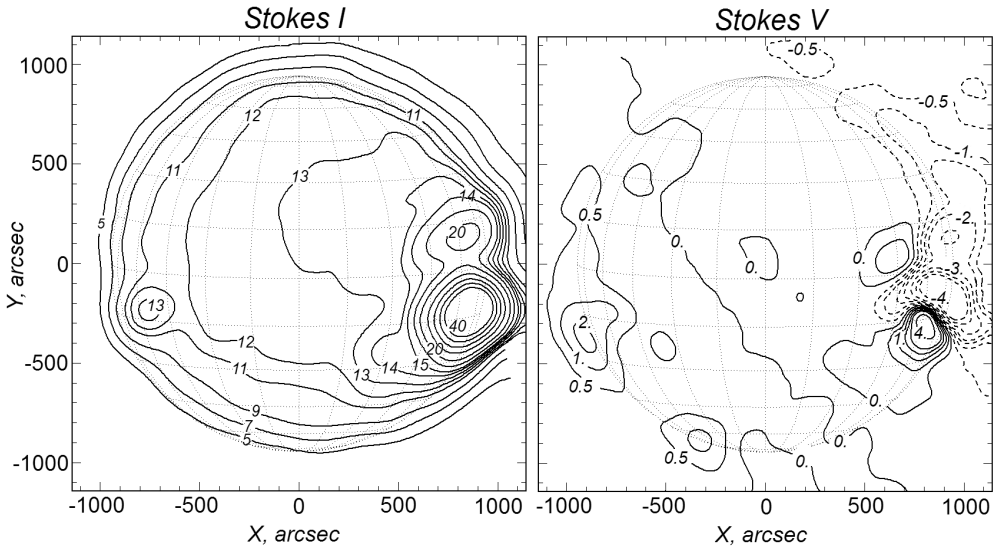

Fig.2. *The solar emission Stokes I and V parameter maps at the 3.76 cm wavelength observed by the RT-32 VIRAC radio telescope on 2012, July 17 UT 7:15. Contours indicate 10^3 K. The V map solid line contours correspond to RCP and dashed ones to LCP (Bezrukovs 2013).*

The total radio flux of the Sun is defined as the sum of the right and left circular polarization fluxes. The radio fluxes of each map are calculated by the brightness temperature numerical integration over the map taking into account the current pixel solid angle.

Next, we compare the calculated total radio flux over the corresponding maps of the Sun with the daily averaged values of the total radio flux from the Sun measured with the Nobeyama Radio Polarimeter (NoRP) (Nakajima et al. 1985). The total radio flux observed at 3.75 GHz and 9.4 GHz by means of the NoRP are linearly interpolated for the spectral polarimeter observation wavelengths.

Some corrections of the quiet Sun brightness temperature are needed for the coincidence of the calculated radio flux and the total solar radio flux observed by the NoRP (Table). The correction factor is not far then some percent from 1. As the daily variations of the total fluxes are of some percents, we conclude that the correction factor in the range of 1.01 – 1.1 is acceptable to enhance the adopted quiet Sun brightness temperatures (determined for the minimum of solar activity in a cycle).

Table. *Some radio brightness correction factors to fit the total radio flux of the Sun*

Date Time (U.T.)	Wavelength	Quiet Sun brightness (Borovik et al., 1992)	Total flux (NoRP) (solar flux units)	Quiet Sun brightness from total flux	Correction factor
16 July 2012 13:19	3.41 cm	12810 K	292.2	13066 K	1.02
17 July 2012 08:10	3.76 cm	13160 K	261.0	13292 K	1.01
18 July 2012 08:05	3.97 cm	13370 K	240.7	13904 K	1.04
18 July 2012 08:05	4.44 cm	14290 K	216.7	16290 K	1.14

5. Deconvolution

The brightness temperature maps of the solar microwave emission have a number of features which require some optimal deconvolution algorithm definitions. The Sun's brightness temperature map structures have a large spatial dimension range from a solar disk size (coronal holes, prominences, large coronal loops) to local source sizes about arc seconds (cores of solar active regions, floculae). The Sun's microwave brightness temperature maps demonstrate a large contrast range in relation to the quiet Sun brightness temperature also. In this sense the solar observations by the RT-32 VIRAC radio telescope need different deconvolution algorithms for the large scale structures and small structures depending on the relative sizes of the source and antenna pattern.

The CLEAN procedure (Hogbom 1974) is known as an appropriate technique for the deconvolution of a set of some separate bright sources. But this procedure suppresses the low contrast sources like coronal holes, coronal condensations, loops and others. The Generalized MEM (GMEM) procedure (Bajkova 1994, Bezrukov et al. 2010) takes advantage of precise deconvolution of alternating brightness in solar maps and it is adopted as the main for the deconvolution of solar spectral polarimetric observations by the RT-32 VIRAC radio telescope.

6. Conclusion

The multichannel spectral polarimetric observations of the Sun by the RT-32 radio telescope require the further development of the observational data processing methods in order to obtain the most precise and adequate information about the Sun's microwave emission.

7. Acknowledgements

This work was supported by the Latvian Council of Science, project Nr.11.1856.

8. References

Bajkova A. T. (1994) Generalized versus classical maximum entropy for imaging. *Proceedings of the 158th International Astronomical Union (IAU) Symposium, held at the Women's College, University of Sydney, Australia, 11-15 January 1993*, Dordrecht: Kluwer, c 1994, edited by J. G. Robertson and William J. Tango., p.215

Bezrukov D. A., Ryabov B. I., Zalite K., Baikova A. T. (2009). Applications of recovering procedures to RT-32 radio maps of the Sun. *Latvian Journal of Physics and Technical Sciences*, v.46, N6, p.49-56.

Bezrukovs D., Ozolinsh G. (2012) The Antenna Pattern of VIRAC Radio Telescope RT-32 at 6 cm Wavelength, *Space Research Review*, Vol. 1, p. 6.

Bezrukov D. (2013). Spectral Polarimetric Observations of the Sun by VIRAC RT-32 Radio Telescope: First Results. *Baltic astronomy*, Vol. 22, N1, pp. 9-13.

Borovik V.N., Kurbanov, M.Sh., Makarov V.V. (1992) Distribution of Radio Brightness of the Quiet Sun in the 2-CENTIMETER to 32-CENTIMETER Range. *Astron. Zh., Vol. 69, pp.1288-1302. (Soviet Astronomy, Vol.36, No. 6/Nov, p. 656)*

Nakajima H., Sekiguchi H., Sawa M., Kai K., Kawashima S. (1985) The radiometer and polarimeters at 80, 35, and 17 GHz for solar observations at Nobeyama. *Astronomical Society of Japan, Publications (ISSN 0004-6264),* vol. 37, no. 1, p. 163-170.

Högbom J. A, (1974) Aperture Synthesis with a Non-Regular Distribution of Interferometer Baselines. *Astronomy and Astrophysics Supplement*, Vol. 15, p.417

MODELING OF SUBSURFACE ICE MANTLE ON INTERSTELLAR DUST GRAINS WITH ASTROCHEMICAL CODE ALCHEMIC (RESEARCH NOTE)

Juris Kalvāns

Engineering Research Institute "Ventspils International Radio Astronomy Center" of Ventspils University College, Inzenieru 101 a, LV-3600, Ventspils, Latvia
e-mail: juris.kalvans@venta.lv

Abstract. Interstellar ices are layers of molecules deposited on fine dust grains in dark and dense molecular cloud cores. Subsurface ice has been considered in a few astrochemical models, which have shown that it can be of great importance.
The aim of this work is to introduce an established subsurface ice description into the state-of-the-art astrochemical model ALCHEMIC. The model has been developed by the Heidelberg astrochemistry group. The result is an up-to-date model for interstellar molecular cloud research with possible application for protoplanetary disks.

Key words: astrochemistry – molecular processes – interstellar medium: clouds, dust, molecules

1. Introduction

1.1. Ices in interstellar clouds

Molecular clouds constitute approximately half of the gas mass in the Galaxy. They undergo fragmentation and gravitational contraction during their evolution. The fragments develop dense and dark cloud cores that are the birth sites of stars in the Universe.

There are several sources of energy in the interstellar medium; interstellar ultraviolet radiation field, cosmic rays (CR), cosmic-ray-induced photons and exothermic reactions are relevant for quiescent molecular clouds. The source of the interstellar radiation that permeates the interstellar medium is hot stars. The dark cores are almost completely shielded from their photons. Cosmic rays are high-energy atomic nuclei that mostly arise in interstellar shocks produced by supernovas (Aharonian et al. 2012). They penetrate even into the most dense cloud cores (Dalgarno 2006). Cosmic rays and secondary electrons excite H_2 molecules in clouds, which produces an internal UV radiation field within the clouds (Prasad & Tarafdar 1983). The dissociation of molecules produces chemical radicals (e.g. free atoms, OH, CH_3, etc.), which in their turn undergo exothermic reactions, both, in gas and solid phases (on dust grains).

The elemental composition of the interstellar medium is approximately 90 % H, 9 % He and 1-2 % heavier elements. Elements heavier than He are loosely referred to as metals. In the clouds, H is in the form of H_2. Refractory metal species constitute the dust. Dust may contain approximately half of metal mass. Molecular cloud cores are dark (extinction of the interstellar radiation field $A_V > 3$) and dense (density of hydrogen nuclei $n_H \geq 10^3$ cm^{-3}). Volatile

species begin to accumulate on the surfaces of the dust grains. They form a layer of ice, major components of which include water, CO, CO_2, and methanol (Öberg et al. 2011). Grain surface and the icy layer are the sites of solid-phase chemistry in interstellar clouds.

The molecules in interstellar clouds are subjected to chemical and physical transformations induced by photons and CRs. They undergo accretion on grains, migration, binary reactions on the surface, photodissociation, and desorption back into the gas phase. The transformations of ice are not limited to the surface. The whole ice layer is subjected to chemical and structural changes due to CRs, CR-induced photons, and exothermic reactions (e.g. Palumbo et al. 2010; Öberg et al. 2010; Accolla et al. 2011).

1.2 Model of interstellar ice mantle

In our previous papers (Kalvāns & Shmeld 2010, 2013, from now on KS2013) a gas-grain astrochemical model for quiescent molecular cloud cores was developed. The model considered the subsurface ice (mantle) phase, which is omitted in many current astrochemical models. It is, perhaps, the first and currently most complete model that attempts to describe the chemical transformation of the subsurface ice. This was done via the concept of closed cavities in the mantle. They are reactive surfaces, isolated from the outer ice surface.

The current model, however, has some drawbacks that have to be solved for better quality results: first, it does not describe the attenuation of interstellar photons properly, even though this is unimportant for molecular cloud cores. Charge exchange between gas and dust particles, anion reactions, stochastic effects for surface reactions are not included in the model either. Besides, the reaction database used (Hasegawa et al. 1992 and Hasegawa & Herbst 1993) is outdated and fails to include several important reactions, particularly, hydrogenation of formaldehyde.

To solve these problems, it was decided to incorporate the mantle-phase chemistry in an existing up-to-date astrochemical model, and not to work on the further development of the program used for Kalvāns & Shmeld (2010, 2013). The model "ALCHEMIC", developed by the Heidelberg astrochemistry group was chosen as the basis for further research. The code was kindly provided by Dmitry Semenov. "ALCHEMIC" utilizes the Ohio State University reaction database[1] (version 2008_03). It includes an extended set of surface reactions, relative to that of Hasegawa et al. (1992); Hasegawa & Herbst (1993). Stochastic effects for surface reactions can be taken into account with the modified rate equation approach (Caselli et al. 1998).

In addition to fixing the above mentioned deficiencies, "ALCHEMIC" will allow to model ice chemistry in protoplanetary disks. Full temperature dependence is included for relevant transformations and reactions of the ice phase. Because of the swap of reaction databases, the new model currently does not include deuterium chemistry. This was an important part of the KS2013 paper. The new model is dubbed "Alchemic-Venta".

2. Rate calculation for processes implemented in "Alchemic-Venta"

The ice mantle model has been explicitly described in KS2013. "ALCHEMIC" is described by Semenov et al. (2010, S2010+). The focus of this paper is on the changes made during implementation of mantle description into the "ALCHEMIC" and their consequences. The

1 Available at Eric Herbst's home page, http://www.physics.ohiostate.edu/eric/research.html

models themselves are not described in detail. In the new model, only processes regarding ice formation and processing have been supplemented or changed.

Some of the changes arise from the fact that the model by Kalvans & Shmeld is designed for cloud modeling, while that of Semenov et al. is mainly for protoplanetary disks. The 'low metal' elemental abundances used by S2010+ were replaced with those used in KS2013, because the latter considers the whole ice mantle, not just its surface. The elements Si, P, and Cl were not considered in KS2013. Their abundances were taken from Jenkins (2009) with $F_* = 1$ for "Alchemic-Venta".

2.1. Accretion

The accretion of species onto grains is significantly faster in KS2013 than in S2010+. Calculations at integration time $t = 1$ Myr with temperature $T = 10$ K and density $n_H = 2\times10^4$ cm^{-3} result in an ice-to-gas abundance ratio of chemically active metal elements C, N, O, and S, which exceeds 100:1 for the former and is approximately 2:1 for the latter model. This is inconsistent with an earlier research, where metal depletion onto grains is expected to occur on the order of 10^5 yr at densities similar to 10^4 cm^{-3} (e.g. Leger 1983).

In the new model the rapid accretion approach was used, as outlined by Willacy & Williams (1993). It results in a much higher rate coefficient. It also takes into account molecule accumulation onto small grains. This allows easy comparison of the results from "Alchemic-Venta" with those from KS2013, because the rapid accretion approach is the one we used in earlier papers.

All the models (Kalvāns & Shmeld 2010; Semenov et al. 2010, and "Alchemic-Venta") consider larger 0.1 μm grains in their physical and chemical description. However, molecule accretion on small grains does not contradict this approach, because the smaller grains coagulate and/or stick onto the larger grains (Köhler et al. 2012).

Positive ions stick to negatively-charged grains some 18 times more efficiently than neutral species (Umebayashi & Nakano 1980; Willacy & Williams 1993). This phenomenon is not described in the original "ALCHEMIC" code. A direct implementation of this process into the model, with the grains neutralized upon each accretion event, has resulted in mostly neutral grains. This seriously alters the ionization fraction. Charge balance may profoundly affect the chemical composition of the gas phase (Kalvāns & Shmeld 2012).

It has been decided not to include this process in the current simulations, in line with S2010+ and KS2013, until a more detailed investigation has been made. The interaction between electrons and grains has been retained 'as is' in "ALCHEMIC".

2.2. Desorption

All desorption mechanisms considered in KS2013 were transferred to "Alchemic-Venta". Evaporation and desorption due to whole-grain heating by direct CR hits was retained exactly as described in S2010+. Desorption by the interstellar radiation field and by CR-induced photons is included, following Roberts et al. (2007). The Habing field (10^8 $cm^{-2}s^{-1}$) is taken as the flux of interstellar UV photons (this mechanism was not included in KS2013). Desorption by the energy released from the reaction H + H on grain surfaces was included in line with Roberts et al. (2007), too. The only mechanism that directly transports subsurface mantle molecules into the gas is impulsive ejection of molecules by cosmic rays passing through the grain (Johnson et al. 1991). For the sake of completeness, it was included in both, surface and

mantle phases in "Alchemic-Venta". In KS2013 it was considered for the mantle phase, only. It should be noted that, according to the current understanding, the yield (or efficiency) for all non-thermal desorption mechanisms is unknown, at least within an order of magnitude (see e.g. Roberts et al. 2007).

Selective desorption of important mantle species greatly affects the abundance of elements in gas and solid phases. Table 1 shows that the ice-to-gas abundance ratio for different elements may differ by orders of magnitude. This ratio is dependent on the ability for an element to storage itself into simple and sticky molecules, such as H_2O or SiO. The atoms of the metallic elements have very high desorption energies.

Table 1. *Total ice-to-gas abundance ratio for metal elements after integration time t = 2 Myr.*

Element	C	N	O	Si	S
ice/gas	6.00E+01	7.50E+00	2.30E+02	3.30E+04	6.40E+02
Element	Fe	Na	Mg	Cl	P
ice/gas	9.60E+03	7.00E+03	2.50E+04	3.60E+04	2.00E+03

2.3 Transitions solid species between phases

The exchange of intact metal molecules between the three ice phases (surface, mantle and cavities) consist of six transitions in total. This is an extension over KS2013, where direct surface-cavity transition was not considered. The relative rates of these processes determine the structure of the mantle. It is characterized by (1) the outer surface area or porosity (Sect. 3.4. in KS2013) and (2) the amount of reactive species within the mantle (on surfaces of closed cavities, Sect. 4.1., KS2013). The desired mantle-to-surface (*M/S*) and mantle-to-cavity average abundance ratios both are assumed 100:1.

The rate coefficients for transitions between the ice phases were calculated as specified in KS2013, Eqs. 16-18. They are assumed to be bound to the rate of the energetic cosmic-ray iron nuclei passing through the grains. In "Alchemic-Venta", the rate coefficients were taken to be 10 times higher. This produces more rapid transition of surface species into the mantle and cavity phases. Physically, this means that the mantle is compacted from porous to dense structure 10 times faster. This is more consistent with the recent experimental results, which revealed that water ice formed on surface at 10 K is compact, not porous (e.g. Linnartz et al. 2011).

With these coefficients $M/S \approx 100 : 1$ is reached in an integration time of approximately 2 Myr. *M/S* may slightly differ between the elements.

2.4 Binary reactions on grains

The calculation of the rate of binary reactions was retained exactly as described in S2010+. The improvements over KS2013 include an extended reaction set, which can be used with higher or lower molecule binding energies. The modified rate equation approach for surface reactions is an interesting and valuable addition because of its possible application in calculating reaction rates for cavity reactions. Cavity surface reactions themselves were

implemented into "Alchemic-Venta" in line with Kalvāns & Shmeld (2010). The relevant parameters are given by KS2013.

2.5 Photodissociation of molecules in ice

The "ALCHEMIC" reaction file includes a set of photoreactions for surface molecules. Both, interstellar and CR-induced photons are considered.

These photoreactions were applied to mantle and cavity species, too. The dissociation yields are provided in the Table 2 of KS2013. It is assumed that H and H_2, split off from surface species, escape into the gas phase (Hartquist & Williams 1990; Kalvāns & Shmeld 2010). They include photodissociation of cavity molecules and mantle molecules. The products of the latter transit to the cavity phase with 1 % efficiency. In addition, the opposite process was introduced in "Alchemic-Venta" – the transition of cavity molecule dissociation products into the inert mantle phase. The efficiency of this process was initially assumed 10 % of the 'traditional' dissociation in cavities. This process was introduced to reflect the trapping of radicals in ice (Öberg et al. 2010).

Photodissociation may initiate the migration of radicals along the depth of the mantle over several monolayers (Andersson & van Dishoeck 2008). Because of this, a bi-directional transition between the phases for the dissociation products in outer-surface and mantle phases was introduced here. It was assumed that the transition of UV or CR-induced photodissociation products from surface to mantle phases, or vice versa, occurs with 1 % efficiency relative to dissociation of molecules in the respective phases without a change of phase.

The real efficiencies of the dissociative reactions with transition between phases are unknown, and can be adjusted if such a need arises. The transition between outer-surface and cavity phases was not considered, because cavities, by definition, are isolated from the surface by at least several monolayers. Molecule exchange directly between cavities and surface can be induced by more energetic events, only (see above). They can be cosmic-ray hits or decay of radioactive nuclei in the grain.

2.6 The diffusion of hydrogen

H and H_2 have a different and more effective phase transition mechanism than other species – diffusion through the lattice of the ice. This process was included in the manner outlined by Kalvāns & Shmeld (2010, 2013).

A simple temperature dependence for hydrogen diffusion coefficient D (cm^2s^{-1}) was introduced, with an Arrhenius equation of type:

$$D = D_0 e^{\frac{E_{act}}{T}}, \quad (1)$$

where E_{act} (K) is the activation energy for diffusion (Strauss et al. 1994). The parameters D_0 and E_{act} for H_2 were calculated from data supplied by Strauss et al. (1994) (at 25 and 43 K; Kalvāns & Shmeld 2010). For H the diffusion coefficients at 10 K (Awad et al. 2005) and 20 K (Strauss et

al. 1994) were used. Such a single-equation temperature dependence with interpolation or extrapolation of limited data sets does not seem to be entirely correct. However, it makes the model more versatile with possible calculations for slightly elevated grain temperature. With this addition, now all relevant processes in the new model are temperature dependent.

There are four ice-phase transition processes in "Alchemic-Venta". First, the CR-induced transition of intact molecules between all three phases is the dominant one. The second process is CR-induced photodissociation that connects the phases according to sequence: surface ↔ mantle ↔ cavities. Molecule dissociation by UV photons works in a similar manner but is much less important because of extinction of the interstellar radiation field in the clouds. The final phase transition is the diffusion of H and H_2. This mechanism is important for determining mantle composition, however, it affects free hydrogen, only.

3. Results

An updated, comprehensive astrochemical model has been created by the fusion of the idea proposed by Kalvāns & Shmeld and the code provided by Semenov et al. (Heidelberg astrochemistry group). The new model "Alchemic-Venta" has some extensions and improvements over the model used in KS2013. They include temperature dependence in all the processes, and extended surface reaction database. These have to be utilized and evaluated during a further research. The calculation time on a modest workstation PC (Intel Core Duo 2.33 GHz CPU, 2 GB RAM) for "ALCHEMIC" is approximately 7 seconds, but "Alchemic-Venta" typically runs for 1-2 minutes. The model has no deuterium reactions within its current database.

Table 2. *Comparison of calculated abundances with observational data. The final (3 Myr) result calculated in Kalvāns & Shmeld (2013), observational results of a high-mass protostar W33A and cloud core Elias 16 are compared to the new results of "Alchemic-Venta" (integration time 2 Myr). The latter results are presented with molecule adsorption energies E_b given as fraction of the desorption energy E_D.*

	KS13	0.33 E_D	0.33 E_D, MRE[a]	0.77E_D	W33A[b]	Elias 16[b]	Low-mass protostars[c]
H_2O	100	100	100	100	100	100	100
CO_2	112	29	31	7	13	18	29
CO	7	7	8	20	8	25	29
CH_3OH	~ 0	19	19	17	18	< 3	5

[a] Modified rate equation approach

[b] Chang et al. (2007)

[c] Öberg et al. (2011)

A short glimpse of the initial results (Table 2) with the given input parameters looks very promising. H_2O, CO_2, and CO have mantle abundances in proportions comparable to interstellar ices (e.g. Öberg et al. 2011). Hydrogenated CO is overproduced, although not to such a high extent as in KS2013. It should be noted that it is methanol, not formaldehyde, that is its main form, which is a significant improvement thanks to the extended surface reaction set. H_2CS is the main sulfur molecule in ice. H_2S, SO, SO_2, and OCS all have high and

similar abundances. The major molecules for nitrogen are ammonia, N_2, HCN, HNCO, HNC, and NH_2CHO. Multi-atom organic species have high abundances, too. These are interesting results and major improvements over Kalvāns & Shmeld (2010, 2013). They pave the way for exploring the chemical role of the subsurface ice layers in a much better quality than before. A useful conclusion is that the reaction database is sufficient for mantle chemistry and does not need immediate extension. This is true at least for the major elements: C, N, and O.

In the above paragraph, the results with low diffusion energy barrier for surface reactions are considered (see Sect. 2.4. of S2010+). They can be directly compared to our previous results, however, the modified rate equation approach is more realistic. Simulation with the modified rate equations approach produces results fairly similar to those described above (Table 2). High diffusion energy (E_b = 0.77 E_D) for surface species results in severe underproduction of CO_2 (Ruffle & Herbst 2001), while methanol is seriously overproduced. One can conclude that the modified rate equation approach is the best option, at least, when the model initial set-up is used, with parameters derived from KS2013 and given in this paper.

The presented results on ice composition are mostly the product of the well-developed "ALCHEMIC" model and OSU reaction database. The introduction of mantle chemistry is beneficial because it enhances the abundance of CO and CO_2 and helps to diminish the overproduction of methanol.

4. Conclusions

The exact values of the various efficiency parameters used in astrochemical modeling are often poorly known. The efficiency of all phase changes (accretion, desorption, ice re-cycling) as well as the photodissociation yield of ice species can be significantly altered within the frame of current knowledge. For example, there is a striking difference when the accretion rate is calculated either as outlined in Willacy & Williams (1993) or S2010+. Other parameters, such as integration time, temperature of gas and dust, cloud density, and extinction of the interstellar radiation field can be adjusted, too. The surface chemistry can be adjusted by changing the approach of doing calculations (simple rate equation, modified rate equations, slow diffusion, Monte Carlo random walk), or editing the reaction list.

The parameters in a model can be adjusted for the simulation results to fit the observational data. In such a way, a single model can account for a variety of cloud and protostar observations. This blessing comes also with the curse that a weak and incomplete model can be adjusted to produce seemingly correct results for a particular case. In many cases this can be done by adding or removing specific chemical reactions that are necessary for achieving the desired result. One has to be very careful when drawing conclusions from the results of models modified in a specific way.

Model results (calculated abundances) can be heavily dependent on the rates of a few phase-change processes and chemical reactions for a few major molecules. This was countered in two ways. First, a wider variety of phase change mechanisms (more than one mechanism for each transition, if physically feasible) in addition to conservative desorption yields were used. Second, the interpretation of results for the solid-phase species was done by drawing general trends. These include abundance ratios for elements in different phases. Especially, this regards the content of chemically bound hydrogen and deuterium.

5. References

Accolla, M., Congiu, E., Dulieu, F., et al. 2011, Physical Chemistry Chemical Physics, 13, 8037
Aharonian, F., Bykov, A., Parizot, E., Ptuskin, V., & Watson, A. 2012, Space Sci. Rev., 166, 97
Andersson, S. & van Dishoeck, E. F. 2008, A&A, 491, 907
Awad, Z., Chigai, T., Kimura, Y., Shalabiea, O. M., & Yamamoto, T. 2005, ApJ, 626, 262
Caselli, P., Hasegawa, T. I., & Herbst, E. 1998, ApJ, 495, 309
Chang, Q., Cuppen, H. M., & Herbst, E. 2007, A&A, 469, 973
Dalgarno, A. 2006, Proceedings of the National Academy of Science, 103, 12269
Hartquist, T. W. & Williams, D. A. 1990, MNRAS, 247, 343
Hasegawa, T. I. & Herbst, E. 1993, MNRAS, 261, 83
Hasegawa, T. I., Herbst, E., & Leung, C. M. 1992, ApJS, 82, 167
Jenkins, E. B. 2009, ApJ, 700, 1299
Johnson, R. E., Donn, B., Pirronello, V., & Sundqvist, B. 1991, ApJL, 379, L75
Kalvāns, J. & Shmeld, I. 2010, A&A, 521, A37
Kalvāns, J. & Shmeld, I. 2012, Baltic Astronomy, 21, 447
Kalvāns, J. & Shmeld, I. 2013, A&A, 554, A111 (*KS2013*)
Köhler, M., Stepnik, B., Jones, A. P., et al. 2012, A&A, 548, A61
Leger, A. 1983, A&A, 123, 271
Linnartz, H., Bossa, J.-B., Bouwman, J., et al. 2011, in IAU Symposium,
Vol. 280, IAU Symposium, ed. J. Cernicharo & R. Bachiller, 390–404
Öberg, K. I., Boogert, A. C. A., Pontoppidan, K. M., et al. 2011, ApJ, 740, 109
Öberg, K. I., van Dishoeck, E. F., Linnartz, H., & Andersson, S. 2010, ApJ, 718, 832
Palumbo, M. E., Baratta, G. A., Leto, G., & Strazzulla, G. 2010, J. Mol. Struct., 972, 64
Prasad, S. S. & Tarafdar, S. P. 1983, ApJ, 267, 603
Roberts, J. F., Rawlings, J. M. C., Viti, S., & Williams, D. A. 2007, MNRAS, 382, 733
Ruffle, D. P. & Herbst, E. 2001, MNRAS, 324, 1054
Semenov, D., Hersant, F., Wakelam, V., et al. 2010, A&A, 522, A42 (*S2010+*)
Strauss, H. L., Chen, Z., & Loong, C.-K. 1994, Journal of Chemical Physics, 101, 7177
Umebayashi, T. & Nakano, T. 1980, PASJ, 32, 405
Willacy, K. & Williams, D. A. 1993, MNRAS, 260, 635

THE ASTROID SIMULATOR SOFTWARE PACKAGE: REALISTIC MODELLING OF HIGH-PRECISION HIGH-CADENCE SPACE-BASED IMAGING

P. Marcos-Arenal[1], W. Zima[1], J. De Ridder[1], R. Huygen[1], C. Aerts[1,2]

[1]Instituut voor Sterrenkunde, KU Leuven, Celestijnenlaan 200D, 3001 Leuven, Belgium
[2]Department of Astrophysics, IMAPP, Radboud University Nijmegen, 6500 GL Nijmegen, The Netherlands

Abstract. The preparation of a space-mission that carries out any kind of imaging to detect high-precision low-amplitude variability of its targets requires a robust model for the expected performance of its instruments. This model cannot be derived from simple addition of noise properties due to the complex interaction between the various noise sources. While it is not feasible to build and test a prototype of the imaging device on-ground, realistic numerical simulations in the form of an end-to-end simulator can be used to model the noise propagation in the observations. These simulations not only allow studying the performance of the instrument, its noise source response and its data quality, but also the instrument design verification for different types of configurations, the observing strategy and the scientific feasibility of an observing proposal. In this way, a complete description and assessment of the objectives to expect from the mission can be derived.

We present a high-precision simulation software package, designed to simulate photometric time-series of CCD images by including realistic models of the CCD and its electronics, the telescope optics, the stellar field, the jitter movements of the spacecraft, and all important natural noise sources. This formalism has been implemented in a software tool, dubbed ASTROID Simulator.

1. Introduction

The ASTROID Simulator is a software package for realistic modeling of high-precision high-cadence space-based imaging observations of a selected stellar field. It permits to estimate the impact of instrumental and natural noise sources to predict the quality of data and the performance of the instrument.

This tool has been designed to perform simulations for a large range of different set-ups thanks to its flexibility and an extended set of input parameters; the ASTROID Simulator is built to be applicable to space missions with a wide range of detector characteristics. The simulator is currently considering charge coupled device (hereafter CCD) simulations but has been redeveloped in a modular architecture that easily allows modifications and implementation of new functionalities, so it can be used for different kinds of future missions with straightforward modifications.

In order to accomplish the multi-mission task, the simulator has been constructed based on two main ideas: employing an architecture based on modularity principles and mimicking a standard science imaging pipeline. The modularity permits to treat any of the steps in the processing independently, and add or modify the implemented functionalities. Any

inexperienced user can easily improve the comprehension of the process due to the standard pipeline architecture. The standard pipeline architecture also makes the access to the source code lighter. For users who want to adapt this simulator to particular space missions, it is easy to identify whatever step in the process is different or has any different feature than those of the present standard regular processing.

A photometry module has been implemented to analyze the simulations. This module analyzes every image generated in the CCD processing module to obtain photometric fluxes and compares the input star catalogue sources with the sources obtained in the produced images. This is described in detail in Sect. 4.

The ASTROID Simulator is based on the original PLATO Simulator (Zima et al. 2010) which was developed for the assessment study of the PLATO M3 mission candidate within ESA's Cosmic Vision 2015-2025 programme. The ASTROID Simulator has been redesigned and implemented as a multi-mission imaging simulator aiming the ease of including new functionalities and detectors. Catala (2011), Claudi (2010) Rauer et al. (2011) provide detailed descriptions of the PLATO mission. The PLATO Simulator, in turn, is based on pre-existing codes that were developed for the ESA Eddington mission candidate (Arentoft et al. 2004; De Ridder et al. 2006).

2. Design

Modularity principles lead to a design where each effect to be applied is separated in a different module so that it can be easily accessed and modified. Each of the noise effects applied to the image is generated in a different "Processing Step" module, containing the algorithm implementation in separated classes. The whole system is structured in separated components, being the "Processing Steps" one of them.

Modular design facilitates the processor architecture, separating the processing itself in three different components named "Preprocessing", "Processing" and "Postprocessing". Besides these components, there is a "Manager" module in charge of triggering, monitoring and controlling the whole system and a DataSet containing the images and processing parameters. Figure 1 shows an overview of the architectural design.

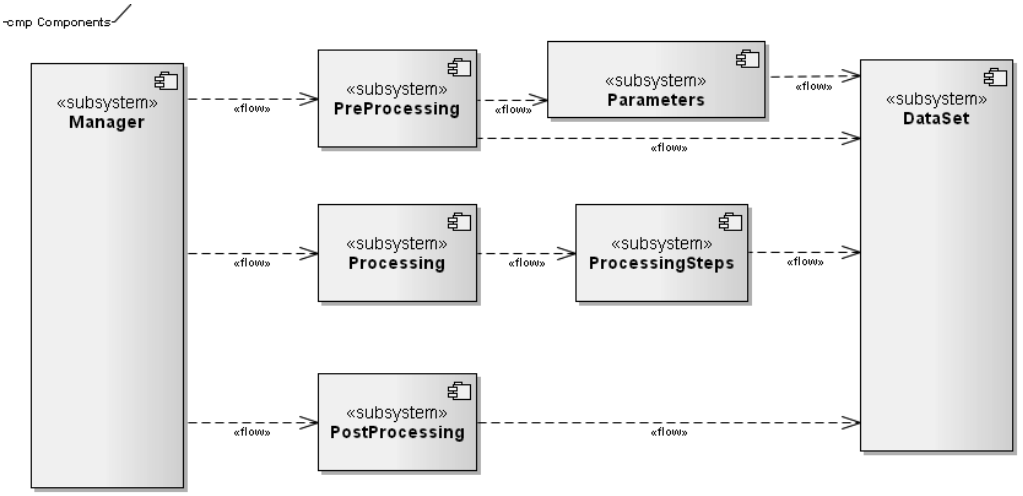

Fig. 1. *Architectural design components relationship overview*

The type of processing to be performed is defined in the "Manager" component depending on the simulation selected by the user (CCD, CMOS, Photometric flux extraction,...). According to this selection, different classes are triggered in the "Preprocessing", "Processing" and "Postprocessing" subsystems.

The input parameters are defined in an XML-file and are structured according to their function in the simulator, e.g. Satellite, Telescope, Stellar field, CCD, or PSF.

The "Preprocessing" component is in charge of preparing the system for the processing. This implies that the "Preprocessing" subsystem reads all the input files and makes sure that all CCD/CMOS and any other parameters required by any of the processing steps (included in the "Processing Steps" component) are included in the DataSet.

As a part of the "Preprocessing" subsystem, we have included the "Parameters" component. This component performs all the calculations indicated by the "Preprocessing" subsystem to set the parameters required for the simulation into the DataSet. These parameters, related to the detector, the star field or any other parameter shared between exposures, are calculated in advance to the processing itself and loaded in the DataSet in order to avoid repeating blocks of code and save processing time. The parameters to be calculated in the "Parameters" component are determined by the Controller depending on the simulation to be performed. Given the CCD simulation example, the Parameters class to be used is the ParamsCCD. This class defines all the properties of the CCD, initializes the sub- and normal-pixel maps and contains methods and algorithms for dealing with the physical and electrical properties of the CCD.

The DataSet module contains all the parameters required to perform the simulation and all the image maps. This includes from the input parameters read in the beginning of the simulation and the calculated parameters employed in the processing, to the final simulated images. This is intended to ease the access to each of the variables and intermediate product or image, in order to analyze every the processing step and its algorithms.

The "Processing Steps" component includes all the noise effects required in the simulation. Each of the effects is deployed in a different module, corresponding to a different step of the processing in such a way that different configurations may use each of the modules separately according to the needs. Figure 2 shows a call diagram including the "Processing" component and the classes implemented in it. As an use case example, the ProcessingCCD class calls every module in the "Processing Steps" component (and so does e.g. the ProcessingCMOS) as all the noise sources are intended to be applied in the baseline processing, but the ProcessingCCD class can easily be modified to leave out any of the noise sources. In the same way, new processing step modules can be implemented and added to any configuration process with a minor impact on the rest of the system. This modular design is a key factor in the design in order to aim for easy usability of this package for other missions.

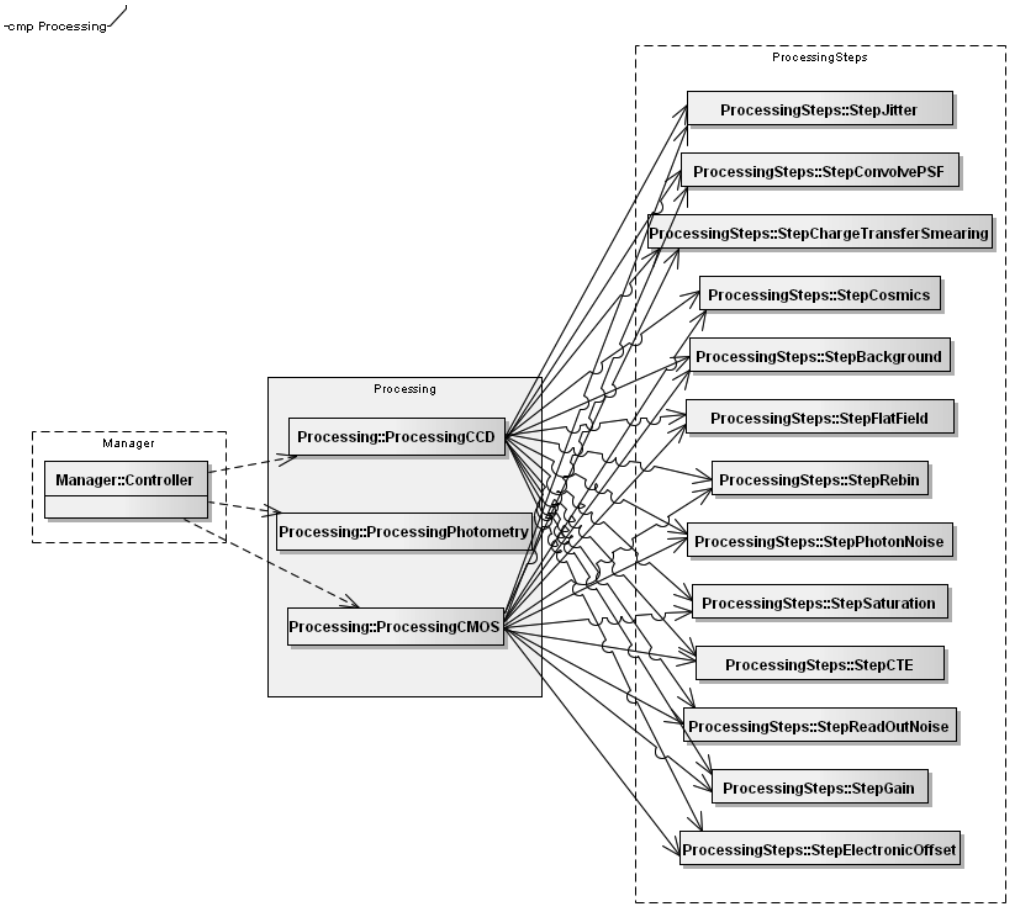

Fig. 2. *Processing call diagram showing different simulation configurations using the same "Processing Steps" modules mimicking a pipeline (top to bottom).*

The Photometry module (ProcessingPhotometry component in Figure 2) is a different type of processing designed to analyze the image products generated in the CCD (or CMOS) processing. When the simulation process is configured to perform the photometry processing (through the Controller component as indicated in the input configuration), the ProcessingPhotometry is called in order to analyze the generated images by photometric algorithms and statistical tools to estimate the noise properties of the data.

The main functionality of the "Postprocessing" component is to write to files the generated images and the required output parameters to disk. The required output is read from the DataSet module. Some external libraries might be required to write these datasets to disk.

3. Imaging model

To model the synthetic image of a science detector, one must take into account a set of parameters in order to ensure obtaining a realistic effect of the implicated noise sources. As a basic initial step, one must define the field of view (hereafter FoV) and take as input parameters the CCD size, number of pixels, pixel scale and project the position of the input star catalogue

into this FoV. In order to accomplish computational requirements, only a part of the image is simulated and the obtained sub-field image results are extrapolated to the rest of the frame.

To increase the simulation accuracy, the calculations are applied at subpixel level. This means that each pixel is represented by a squared map of subpixels to take into account the intra-pixel sensitivity of the CCD to capture some of the effects such as the jittering (usually movements smaller than the pixel size) and the pixel sensitivity variations - flat field (assuming a 1/f spatial power spectrum which resembles a typical CCD as shown in De Ridder et al., 2006). Once the noise effects modeled at sub-pixel level are applied, the sub-pixels are rebinned back again to the original pixel scale. The processing pipeline corresponds to the "Processing Steps" right column top to bottom in Figure 2.

The PSF degradation is applied to the sub-field image (performing a convolution in the Fourier space) as well as the charge-transfer smearing, the cosmic hits and the sky background. Once the rebinning is applied to the image and is scaled back to the image, the photon noise, full-well saturation, charge-transfer efficiency, read-out noise, gain and the electronic offset effects are applied to the synthetic image as shown in Figure 2.

4. Simulation example and conclusions

Series of simulations have been made to test the performance of the photometric observations of the PLATO mission in some concrete aspects regarding the Jittering noise, PSF and CCD performance. For this task, we used a star catalogue of one of the proposed FoV of PLATO containing more than 32000 sources with $m_v \leq 15$ (Barbieri et al. 2004). As an example of one of the assessment simulations made in the performance test, we show the simulation of one-week of observations time-series, corresponding to 24,192 exposures, which have been computed and analyzed using the photometric algorithms for the assessment of the concrete input conditions of the mission. Figure 3 presents an output of the analysis features of this simulation. It shows the obtained magnitude for each source detected with the photometry algorithms in the output synthetic images as a function of the magnitude of the same sources in the input star catalogue. The degradation in performance due to noise as a function of the magnitude is represented. In this plot, the sources with input $m_v \leq 9$ present measured magnitude brighter than the input magnitude since the flux of other stars leaks into the photometry mask.

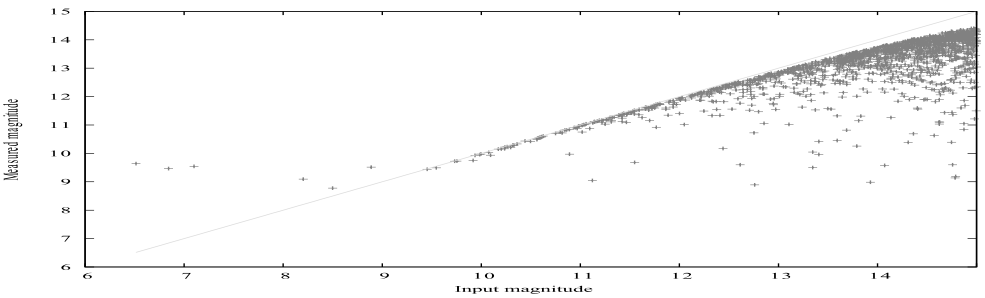

Fig. 3. *Magnitude of the stars in the generated synthetic images as measured with the photometric process as a function of the input magnitude given in star catalogue. The green line indicates the measured magnitude equal to the input magnitude.*

In the future, we plan to expand the simulator modalities and perform various sets of simulations along with their analysis as illustration of the capabilities of our software package.

5. Acknowledgement

The research presented here was based on funding from the European Research Council under the European Community's Seventh Framework Programme (FP7/2007--2013)/ERC grant agreement n°227224 (PROSPERITY) and from the Belgian federal science policy office Belspo (C2097-PRODEX PLATO Science Development).

6. References

Arentoft, T., Kjeldsen, H., De Ridder, J. & Stello, D. (2004). The Eddington CCD data simulator. Second Eddington Workshop: Stellar structure and habitable planet finding, 9 - 11 April 2003 (59 - 64). Palermo, Italy. F. Favata, S. Aigrain and A. Wilson. ESA SP-538, Noordwijk: ESA Publications Division, ISBN 92-9092-848-4.

Barbieri, M. et al. (2004). Search for an optimal Eddington Planet Finding Field. Second Eddington Workshop: Stellar structure and habitable planet finding, 9 - 11 April 2003 (59 - 64). Palermo, Italy. F. Favata, S. Aigrain and A. Wilson. ESA SP-538, Noordwijk: ESA Publications Division, ISBN 92-9092-848-4.

Catala, C. (2008). PLATO: PLAnetary Transits and Oscillations of stars. *Experimental Astronomy*, *23* (1), 329–356. DOI: 10.1007/s10686-008-9122-9

Catala, C. & Appourchaux, T. (2011). PLATO : PLAnetary Transits and Oscillations of stars. *Journal of Physics: Conference Series*. *271* (1), 012084. DOI:10.1088/1742-6596/271/1/012084

Claudi, R. (2010). A new opportunity from space: PLATO mission. *Ap&SS*. *328* (1-2), 319–323. DOI: 10.1007/s10509-010-0299-9

De Ridder, J., Arentoft, T. & Kjeldsen, H. (2006). Modelling space-based high-precision photometry for asteroseismic applications. *MNRAS*. *365* (2), 595–605.DOI: 10.1111/j.1365-2966.2005.09744.x

ESA. (2011). *PLATO Defintion Phase Study report RED BOOK*. Noordwijk: ESA Publications Division.

Rauer, H. & Catala, C. (2011). The PLATO mission. *Proceedings of the International Astronomical Union*. *6*, 354–358. DOI: 10.1017/S1743921311020436

Zima, W. *et al.* (2010). The PLATO End-to-End CCD Simulator -- Modelling space-based ultra-high precision CCD photometry for the assessment study of the PLATO Mission. 4th HELAS International Conf.: Seismological Challenges for Stellar Structure, 1-5 February, 2010. *793*, 5.

SUBJECTIVE VIDEO QUALITY ASSESSMENT METHODS

R. Pauliks[1,2], K.Tretjaks[1], K.Belahs[1]

[1] Engineering Research Institute "Ventspils International Radio Astronomy Centre" of Ventspils University College, Ventspils, Latvia
[2] Faculty of Electronics and Telecommunications, Riga Technical University, Riga, Latvia
*Corresponding authors email: romass@venta.lv

Abstract. Since digital video technology has been replacing analog technology, SDTV coexists with HDTV, 2D TV coexists with 3D TV a variety of technical standards (video display and signal formats, analog and digital video interfaces, video compression ratio levels and wired and wireless transmission technology) has increased. A great number of choices of video encoding and transmission technology technical specifications with different video content quality are possible. Technical improvements and development of new technology does not always match with a high level of observer's subjective assessment of video quality.
There are a lot of subjective video quality assessment methods (SSNCS, SSCQE, DSCQS, DSIS, PC, ACR, etc.) for a wide variety of applications (digital TV, video surveillance, object recognition, overall video quality, compression artefacts and transmission technology impairment level, etc.), so they need to be listed, structured and classified. The goal of the paper is a brief survey of measurement methods for subjective video quality assessment. Firstly, the methods classification is given, secondly, a generalized analysis of crowd-based questionnaire measurement data (1265 observers, 738 women and 527 men, aged from 11 to 85) is presented. The results show that most observers preferred two-screen double stimulus as a simpler and more comfortable method compared to one-screen single stimulus method, but in contrast statistical calculations show that there is a very strong correlation (0,93) between the both methods. In the future research it is necessary to measure experimentally and analyse which of these methods are statistically most reliable and repeatable.

Key words: Subjective Video Quality, Video Quality Testing, Measurement and Assessment.

1. Introduction

Nowadays we have many digital television standards (DVB-T/S/C/H, IPTV) that use wired and wireless transmission technologies and protocols (IP, RTP, RSTP, DASH, HTTP, HTLML5), several encoding/decoding standards (MPEG-2, H.264/AVC, HEVEC), as well as different displays (LCD, LED) varying in size (16:9, 720p, 1080i/p), technology and interface (SDI, ASI, CVBS, YPbPr, HDMI) standards. There are a lot of configuration options for encoding, multiple choices of encapsulation and transmission, etc. All of the abovementioned influence technical quality of video displayed and also objective and subjective assessment of video quality made by a viewer. New and improved video encoding and transmission technology (e.g.

HEVEC, HTTP/HTML5, WebM, Theora, VP8) are clearly required to adapt and improve existing objective video quality measurement algorithms (e.g. PSNR, SSIM, VQM) and verify algorithms with redesigned subjective video quality measurements (e.g. PC, ACR, DCR, DSIS).

The given paper is organized as follows: The second section covers a detailed description of subjective video quality assessment methods and rating scales. In the third section there are briefly described the crowd-based video quality measurement process. The last part of the paper consists of processing, analysis and discussion of measurement results and finally conclusions, recommendations, acknowledgement and the list of references.

2. Subjective video quality assessment methods and rating scales

Mean Opinion Score (MOS) is a subjective quality measurement that has been used nowadays in video, audio compression and television broadcasting and streaming technologies to obtain the human user's view of the quality of the encoding and transmission quality. For MOS measurements it is possible to use many video quality assessment methods and rating scales [1, 2, 3, 5, 6]. MOS can be used to assess the overall video quality and the level of video quality impairment assessment [5, 6, 7, 8, 9, 10, 11]. For subjective video quality assessment tests there are normally recruited at least 15-25 observers. In the assessment results, the number of votes by the observers in each category is weighted by the assessment scores and expressed as a Mean Opinion Score (MOS). For video quality impairment tests there is normally used DMOS = assessment video score - reference video score + 5, in case of five-grade scale, they are sometimes called DMOS (Degradation MOS) values.

The section is divided in two subsections. The first subsection covers the description about video quality assessment methods, but in the second subsection there are briefly described video quality rating scales.

Video quality assessment methods

There exist many video quality methods, but it is possible to classify them in three groups: the first group consists of one screen single stimulus methods, the second group consists of one screen double stimulus methods and finally the third group is derived from second group methods and it is used simultaneously on two screens for the same double stimulus methods [1, 2, 5, 6, 7].

Single Stimulus (SS) or Absolute Category Rating (ACR) is a method where the test sequences are presented one at a time and are rated independently on a five-grade (overall video quality) category scale (see Table.2). In special cases it is possible to use Absolute Category Rating-Hidden Reference (ACR-HR) and Single Stimulus with Multiple Repetitions (SSMR).

Single Stimulus Continuous Quality Evaluation (SSCQE) is continuous evaluation method for evaluating overall video quality. Video sequences are presented to the observer only once in randomized video sequence order to minimize the contextual effect. The most common is a hundred-grade (overall video quality) evaluation shown in Table.3 and Fig.3.

Double-Stimulus Continuous Quality-Scale (DSCQS) method primarily was used for performance evaluation. DSCQS may minimize video contextual effect by using an alternate way of presenting the video sequences. DSCQS method is preferred when the quality of the reference and the test video sequences is similar. The most common is a discrete or continuous

hundred-grade (overall or impairment video quality) evaluation presented in Table.3 and Fig.3. In special cases it is possible to use Simultaneous Double Stimulus for Continuous Evaluation (SDSCE) method suitable to evaluate the effect of sparse impairments, such as transmission errors.

Double-Stimulus Impairment Scale (DSIS) is equivalent to Degradation Category Rating (DCR) method, which are usable to measure the robustness of high quality systems. Both methods are useful for evaluating visual impairments, such as blockiness, blurring and ringing, which are the most common failures, caused by the encoding process. The most favourite is a five-grade (impairment video quality) scale Table.2.

The Pair Comparison method (PC) performs a direct one-to-one comparison between two video systems. The purpose of this comparison is to know which system is the best and how much one is better than the other. The most common rating scale used in PC to assess the difference between the first and the second video systems (simultaneously representing left or right) presentations is shown in Table.4. In some cases to assess overall video quality or video quality impairment level between pairs of the video presentations it is possible to use five, nine, eleven or hundred-grade scales shown in Table.2 and Table.3.

For the Subjective Assessment of Multimedia Video Quality (SAMVIQ) and SAMVIQ-Hidden Reference (SAMVIQ-HR) [12] video assessment sequence the number of views are left up to the observers to decide, and since each video evaluation can be assessed while compared and checked, it is expected that this method will produce assessment results that are more reliable and stable. Usually SAMVIQ tests use computer software with special recommended graphical interface where sliders are used in discrete hundred-grade scale presented in Table.3.

In some cases very simple video quality tests are necessary, for example, special tasks, and objects recognition or text readability [3].

Starting from the video encoding, transmission and representation on the viewer's screen it is possible to highlight the degradation of video signal (see Table.1).

Table.1 *Video signal quality artefacts and impairments*

Video signal Encoding and Transmission Impairments	Video signal, interfaces, acquisition and post-processing distortions
Blocking, blurring, colour bleeding, ringing, staircase effect, mosaic effect, mosquito noise, false contouring, false edge, flickering, fluctuation, ghosting, jerkiness, motion compensation mismatch, stationary area fluctuation, smearing and video scaling, picture freeze, etc.	Brightness, contrasts, colour reproduction, background stability, speed in image reassembling, jerkiness, smearing, mosquito, double images/shadows, gamma, luminance, illuminance, etc.

One screen double stimulus and two-screen double stimulus graphically measurement procedure are represented in Fig.1 and Fig.2.

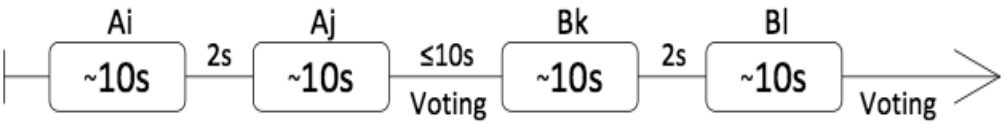

Ai, Aj Sequence A under i^{th} and j^{th} test condition respectively
Bk, Bl Sequence B under k^{th} and l^{th} test condition respectively

Fig.1. *PC (one screen) video quality assessment procedure*

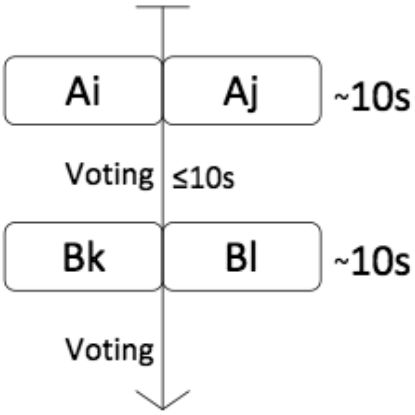

Ai, Aj Sequence A under i^{th} and j^{th} test condition respectively
Bk, Bl Sequence B under k^{th} and l^{th} test condition respectively

Fig.2. *PC (two screens) video quality assessment procedure*

If necessary to measure the quality of the video signals with very low video quality changes, it is advisable to use two screen method with which you can probably easily identify the differences between the reference and impaired video, especially useful for video encoding parameter tuning or two different equipment hardware and software video quality comparison. At the same time two screen method could be a perfect for experts "golden eyes", while one screen method is equally suitable for both experts and ordinary observers, especially in cases where there is need to assess the overall quality of the video coding and transmission system rather than the quality of each individual item separately.

There are some proprietaries or modifications of standardized methods e.g. MSU Continuous Quality Evaluation (MSUCQE), Multiple References Impairment Scale (MRIS), etc.

Video quality rating scales

There exist many video quality rating scales, but it is possible to divide them into few groups, the first group is discrete rating scales, e.g. five, nine, eleven or hundred grade scales and the second group is continuous rating scales, which is usually used in a hundred grade

scales using hardware or software based quality rate slider [4].

In continuous subjective video quality assessment method the observers for voting use a hardware based slider (score recording device). The continuous voting slider has to meet the following conditions: slider mechanism without any sprung position, fixed or desk-mounted position, linear range of travel of 10 cm, video samples recorded twice a second.

Video quality rating scales classifications shown in Table.2, 3, 4 and Fig.3.

Table 2. *Quality and impairment rating scales (five-grade)*

Numerical value	Quality scale	Impairment scale
1	Bad	Very annoying
2	Poor	Annoying
3	Fair	Slightly annoying
4	Good	Perceptible, but not annoying
5	Excellent	Perceptible

Table 3. *Additional quality rating scales (nine, eleven and hundred grade)*

Numerical value	Quality scale (nine grade)	Numerical value	Quality scale (eleven grade)	Numerical value	Quality scale (hundred grade)
		10	*	100	*
9	Excellent	9	Excellent	90	Excellent
8		8		80	
7	Good	7	Good	70	Good
6		6		60	
5	Fair	5	Fair	50	Fair
4		4		40	
3	Poor	3	Poor	30	Poor
2		2		20	
1	Bad	1	Bad	10	Bad
		0	**	0	**

* No further improvement is possible, ** A worse quality cannot be imagined

Table 4. *Rating scales for PC tests*

Numerical value	Quality and Impairment scale	
+3	Much worse	Left video quality is much better than the right video
+2	Worse	Left video quality is better than the right video
+1	Slightly worse	Left video quality is slightly better than right video
0	The same	Both of the same video quality
1	Slightly better	Right video quality is slightly better than left video
2	Better	Right video quality is better than the left video
3	Much better	Right video quality is much better than the left video

Two forms of continuous voting are possible: the scale may include some reference points for the voting or the range of the numbers for all scale (e.g. 0-100), see in Fig.3.

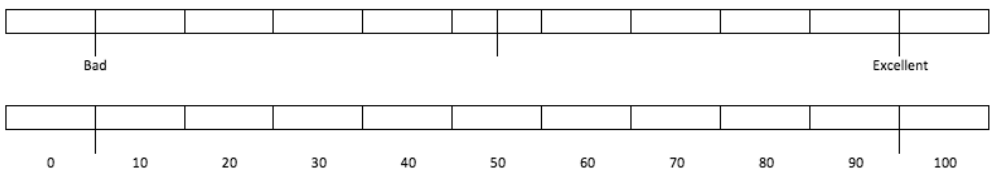

Fig.3. *Rating scales for continuous quality assessment tests*

In some cases it is necessary to use very simple stimulus-comparison procedure to compare original with processed video. For example, in pair performance comparison (text readability, identifying objects (sharpness, contrast, fidelity, colour hue and saturation)) very simple quality scale may be used: 1: Better, 0: The same, -1: Worse.

3. Crowd-based video quality measurement process

The crowdsourcing or crowd-or-cloud-based testing is a virtual video quality measurement technique using web based tools and Internet connection. In some cases it is a very good alternative compared to the expensive and time-consuming laboratory based subjective video quality testing.

Crowd-based questionnaire consists of 10 questions. First is gender, second is age, the next 5 questions are about rating scales and last 3 questions are about one screen doubles stimulus (DS) or two screen simultaneous doubles stimulus methods, see method graphically presented in Fig.1 and Fig.2. Crowd-based questionnaire and measurement results are publically available on skypromo.lv/ipt/ [4].

4. Assessment results processing, analysis and discussion

In the tests involving more than 1300 observers, 1265 tests were found to be valid, completed by 738 women and 527 men, aged from 11 to 85 years with a mean age of 27,56 years.

Video quality assessment results for the same video picture quality rating used different MOS (5, 9, 11 and 100) scales:

For the five grade scale, min=1, max=5, mean=3,949 and std=0,723.

For the nine grades scales, min=1, max=9, mean=7,081 and std=1,434.

For the eleven grade scale, min=0, max=10, mean=7,349 and std=1,616.

For hundred grade scale, min=0, max=100, mean=76,606 and std=17,977.

Statistically insignificant differences were observed between the various assessment scales, but it is highly recommended to diversify the test sequence and combine the use of different rating scales.

Choosing the best rating scale, five-grade scale is the best for 399 observers, nine-grade scale for 97, eleven-grade scale for 117, hundred-grade scale for 280 and any of the offered rating scales is the best for 372 observers.

Statistically we don't see significant differences between one screen and two screen double stimulus methods used for the same video picture quality assessment, e.g. SD mean=13.043, std=21.593 and for the SDS=13.05, std=21.595, but the most of the observers preferred SDS=953 method as simpler and more comfortable, 228 responders accepted both methods and only 84 preferred DS method. See graphical representation in Fig.4 and all test results on a public website [4].

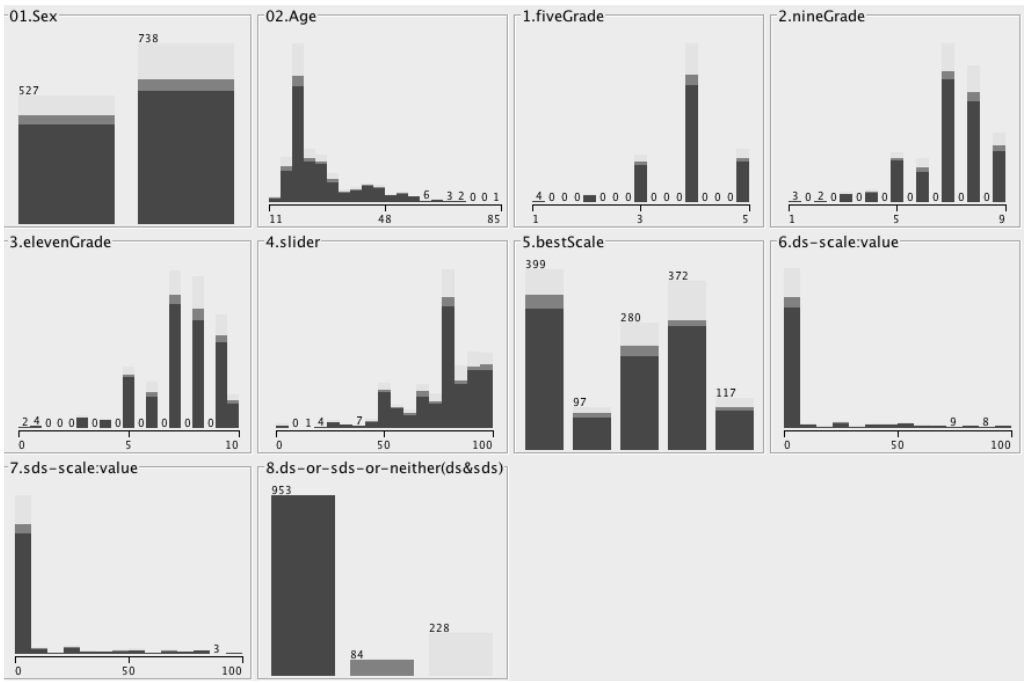

Fig.4. *Crowd-based questionnaire measurement results*

The measurement data show very high correlation coefficient (0,93) between one screen and two screen double stimulus methods (See Fig.5).

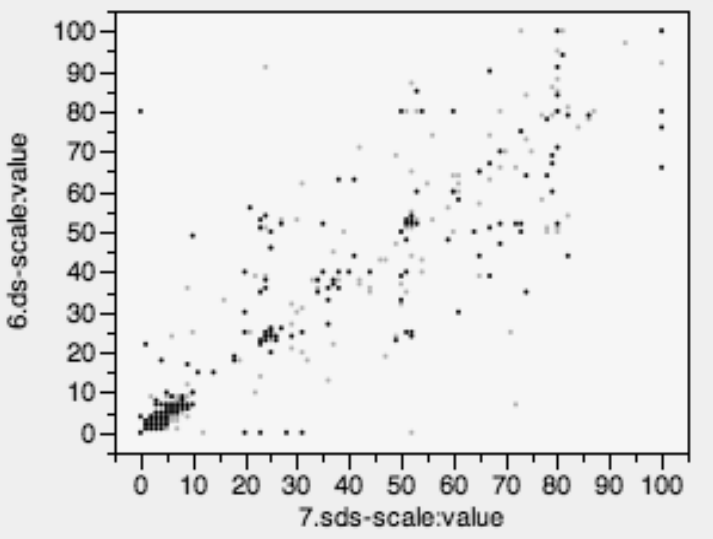

Fig.5. *One-screen vs Two-screen double stimulus measurement results*

The detailed crowd-based measurement result analyses are outside the scope of this paper and are left to other research.

5. Conclusions and recommendations

There are several video quality assessment methods and scales, as well as it is possible to combine these different assessment methods and scales. Crowd-based questionnaire data show that for relatively short tests (2-3min) all video quality-rating scales are equally well suited for both the overall and for the impairment video quality assessment. In very large impairment video sequences tests in case where the distortions are relatively easily to be noticed compared two video quality assessment methods: one screen (DS) and two- screen simultaneous double stimulus (SDS) Pair Compare (PC) methods. The video quality comparison brings to the conclusion that there is a very close correlation between the two methods (0,93), while allowing respondents to choose between methods, 75% of respondents prefer to simultaneously two screens PC SDS method. SDS method is more suitable if necessary to measure relatively small and difficult to perceive video quality impairment changes.

After literature review authors conclude that there is a relatively small amount of research work [13, 14, 15, 16] available which experimentally compare and analyse different video quality testing methods, rating scales and their possible combinations, as well as on the basis of the recommendations should point out which of the methods and rating scales to choose for a specific video quality assessment applications.

Based on the recommendation in the future research it is necessary to measure experimentally and analyse which of these methods are statistically most reliable, repeatable and for what kind of video application is more suitable

.

6. Acknowledgement

This paper is financed from European Regional Development Fund's project "International competitiveness and capacity-building of Satellite research" (SATTEH, No.2010/0189/2DP/2.1.1.2.0/10/APIA/VIAA/019) being implemented in Engineering Research Institute "Ventspils International Radio Astronomy Centre" of Ventspils University College.

7. References

1. Methodology for the subjective assessment of the quality of television pictures. ITU–R Rec. ITU. – Geneva, Switzerland, 2009. BT.500–12–09/2009.
2. Subjective video quality assessment methods for multimedia applications. ITU–T Rec. ITU. – Geneva, Switzerland, 2008. P.910–04/2008.
3. Subjective video quality assessment methods for recognition tasks. ITU–T Rec. ITU. – Geneva, Switzerland, 2008. P.912-08/2008.
4. Crowd-based questionnaire and subjective quality measurement results tables and graphics. SS, DS and SDS measurement results. Online: https://sites.google.com/a/venta.lv/romass/.
5. Subjective picture quality assessment for digital cable television systems. ITU-T Rec. ITU. – Geneva, Switzerland, 1998. J.140–03/1998.
6. Subjective assessment methods for image quality in high-definition television. ITU-R Rec. ITU. – Geneva, Switzerland, 1998. BT.710-4/1998.
7. Subjective assessment of conventional television systems. ITU-R Rec. ITU. – Geneva, Switzerland, 1998. BT.1128-2/1997.
8. Subjective assessment of standard definition digital television (SDTV) systems. ITU-R Rec. ITU. – Geneva, Switzerland, 1998. BT.1129-2/1998.
9. Test materials to be used in subjective assessment. ITU-R Rec. ITU. – Geneva, Switzerland, 1994. BT.802-1/1994.
10. Test materials to be used in assessment of picture quality. ITU-R Rec. ITU. – Geneva, Switzerland, 2012. BT.1210-4/01/2012.
11. Subjective assessment of stereoscopic television pictures. ITU-R Rec. ITU. – Geneva, Switzerland, 2000. BT.1438/2000.
12. Methodology for the subjective assessment of video quality in multimedia applications. ITU-R Rec. ITU. – Geneva, Switzerland, 2007. BT.1788.
13. Pinson M., Wolf. S. Comparing subjective video quality testing methodologies // Proceedings of SPIE: the International Society for Optical Engineering, 2003. – Vol. 5150. – P. 573–582.
14. Lee, C., Choi, H., Lee, E., Lee, S., Choe, J. Comparison of various subjective video quality assessment methods // Proceedings of SPIE - The International Society for Optical Engineering Volume 6059, 2006, Article number 605906.
15. Winkler, S. ON the properties of subjective ratings in video quality experiments // 2009 International Workshop on Quality of Multimedia Experience, QoMEx 2009, art. no. 5246961 , pp. 139- 144.
16. Tominaga, T., Hayashi, T., Okamoto, J., Takahashi, A. Performance comparisons of subjective quality assessment methods for mobile video // 2010 2nd International Workshop on Quality of Multimedia Experience, QoMEX 2010 – Proceedings, Article number5517948, Pages 82-87.

DEVELOPMENT OF DISTRIBUTED REAL TIME DATA ACQUISITION SYSTEM FOR RADIO TELESCOPE MONITORING

K. Ruibys[1,2], A. Andziulis[1,2], T. Eglynas[3], M. Jusis[2], D. Drungilas[1], G. Gaigals[4].

1) Klaipeda University, Department of Informatics Engineering, Bijunu str. 17-206, Klaipeda, Lithuania. E-mail: KRuibys@gmail.com, Arunas.iik.ku@gmail.com, dorition@gmail.com.
2) Klaipeda University, Mechatronics Science Institute Bijunu str. 17, Klaipeda, Lithuania. E-mail: Mindaugas.Jusis@gmail.com.
3) Vilniaus Gedimino Technikos University, Department of Transport Technological Equipment, Plytinės g. 27, Vilnius, Lithuania. E-mail: tmse@inbox.lt.
4) Venspils Augstskola, Faculty of Information Technologies and Engineering Research Institute "Ventspils International Radio Astronomy Centre", Inzenieru 101, Ventspils, Latvia. E-mail: gatisg@venta.lv.

Abstract. One of the most important issues in radio astronomy is data acquisition, ensuring reliable and accurate data processing and information storage for monitoring the complex radio telescope control process. Failures arising in such control process give a significant impact for the entire space data collection system. In order to ensure a continuous monitoring, system performance, increase reliability and accuracy, it is necessary to distribute the system into several independent parts, which in case of failure are able to complement each other and at the same time independently solve a common problem. A distributed real-time data acquisition system is very important when it is needed to connect multiple devices. Moreover, the reliability of the system consisting of divided modules is increased because the failure of one module is limited to the specific functionality. The aim of this work is to propose a conceptual model for developing distributed real-time data acquisition system for radio telescope monitoring. The main advantage of such distributed data acquisition system is that the system can be extended and improved according to the needs. The distributed real-time data collection system model was designed using LabVIEW Datalogging and Supervisory Control (DSC) Module. The system allows real-time monitoring and visual data representation. All collected data is stored in the distributed system database which might be accessed remotely using cloud technology. The paper presents the results that have been obtained in the laboratory using the sensor network as a simulation of the radio telescope. The system analysis showed that the system could be adapted to the radio telescope RT-16 located in Irbene (Latvia).

Keywords: data acquisition, radio telescope, LabVIEW, data recording, distributed system.

1. Introduction

Reliable and accurate data acquisition is one of the most important issues in radio astronomy, especially for monitoring processes of radio telescope control. Future telescopes will have a large number of precision control elements and a large field of view. The distribution

of their control and monitoring systems into several independent parts is important as it ensures continuous monitoring, increased performance, accuracy and reliability. Besides, they can complement each other and solve a common problem at the same time. Distributed measurements provide the user with numerous advantages over more traditional centralised approaches. Distributed data acquisition implementation can greatly simplify the end users' installation and maintenance, allowing connection of multiple devices and providing savings in time and resources. However, while developing distributed measurement systems, the functionalities like internal signal conditioning, excitation, and noise reduction should be improved [1].

Therefore, the aim of this paper is to propose a conceptual model (topological structure, algorithm and LabVIEW capabilities to realize this system) for developing distributed real-time data acquisition system for radio telescope monitoring. Also, it could be adapted to the radio telescope RT-16 located in Irbene, Latvia to ensure efficiency of the entire space data collecting system.

2. Related works

Reviewing the distributed control and monitoring systems applications on radio telescopes [2] is an example of an implementation distributed control system. Such system increases accuracy and operational reliability that can keep the system running without human intervention. Additionally, the usage of measurement instruments of any kind (ranging from large complex equipment to networks of sensors that collectively appear as a distributed measurement device) has become very important in all branches of experimental sciences. Owing to the increasing networking capacity and access ubiquity, distributed system instrumentation is ever more frequently accessed remotely by users who want to perform experiments, collect and process experimental data, analyse and interpret results [3].

As well as appropriate monitoring technology, the distributed data acquisition system plays an important role in large scale of multidimensional data pre-processing and knowledge extraction. As it was shown in experiment (the system which communicates with host unit via CAN bus composed of 36 data acquisition units monitoring cells parameters (Figure 1)) the distributed topology could effectively improve the speed of data acquisition [4].

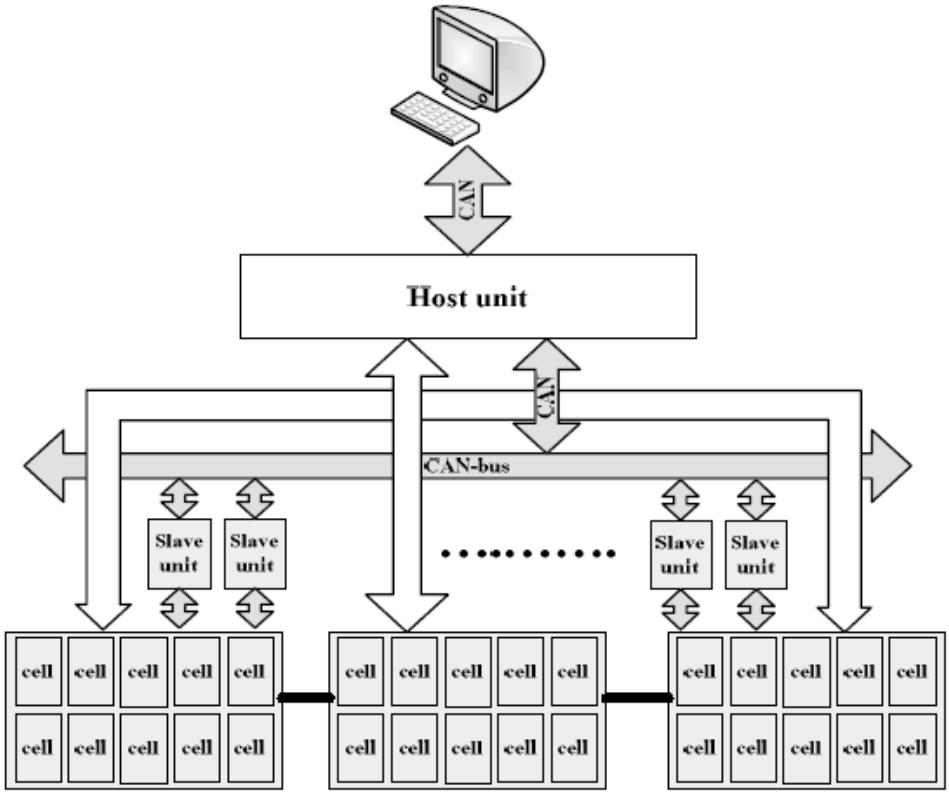

Fig. 1. *The structure of the distributed data acquisition system [4]*

From the technological implementation point of view, the embedded Ethernet and Power over Ethernet (PoE) technology and specific topological structure (Figure 2) allow to implement large-scale data acquisition, real-time information transmission, complex signal processing and intelligent control [5].

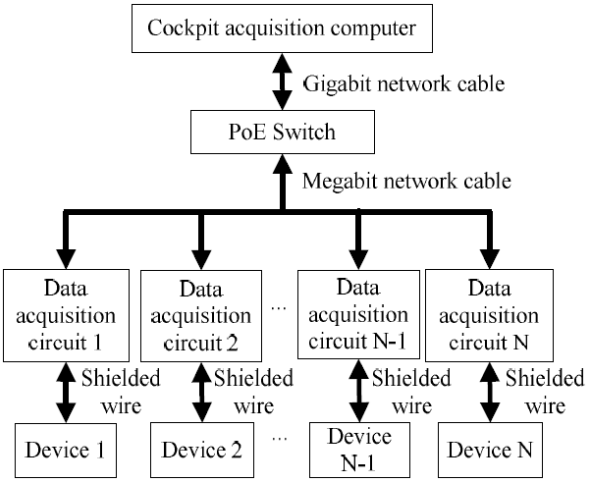

Fig. 2. *The topological structure of distributed data acquisition using embedded Ethernet and Power over Ethernet (PoE) technology [5]*

The distributed data acquisition and control system implementation also depends on software and hardware platforms. There are many examples [6, 7] which demonstrate that development and analysis of distributed systems can be implemented in such modern platforms like cRIO and using LabVIEW software tools.

The advanced and effective system with excellent distributed monitoring ability can be implemented using NI-DAQ and LabVIEW [8]. Moreover, LabVIEW graphical programming environment and hardware containing various distributed sensors are suitable for development of complex systems [9], that can perform not only real-time data acquisition of multiple channels, waveform display, data storage, signal analysis, playback measurement and output printing, etc. [10], but also has good expansibility, high speed and friendly interface. As well as developing a radio telescope monitoring system it can be implemented using a remote module [11] that has data acquisition and is capable to sense temperature, electric current and acceleration of radio telescope actuators. By integrating ZigBee and WEB technologies for remote environment information monitoring and applying LabVIEW virtual instrument platform, the monitoring system can sample real-time environmental information by means of wireless sensor networks and simultaneously transmit it to a PC through RS-232 bus. The information distributing system establishes the connection between the monitoring system and the Internet and transmits the acquired information to the WEB data server [12].

3. Architecture of Distributed Radio Telescope Monitoring System

Considering various distributed system architectures and remote sensing systems, distributed real-time data acquisition system for radio telescope monitoring can be implemented by proposed topological structure as shown in Figure 3. Basically, most of all sensors for radio telescope monitoring are analogue. Therefore, when the system gets signals from the sensors, the analog-to-digital converter should change it to digital data. The first step of digital signal (data) processing could be done locally using National Instruments (NI) hardware (CompactRIO, PXI), in order to decrease the network load. Moreover, usage of distributed system reduces cabling noise, increases reliability and safety, minimizes installation time, simplifies maintenance, and reduces costs associated with cabling and maintenance, in addition to extending system lifetime with a predictive failure method [1]. Also, when we have huge amounts of data, the distributed data processing can be done in multiple devices. It is very important for systems of space signal acquisition and processing. All data are written in TDMS (technical data management solution) file format in National Instruments software (LabVIEW modules and applications). Data are saved in the server and shared for local workstations, other NI hardware and remote clients. The communication between the WSN programmable gateway and measurement nodes works on IEEE 802.15.4 and ZigBee technology. Moreover, these wireless measurement nodes (Figure 3) will be used only in test mode of the system, because wireless networks are prohibited in the vicinity of radio telescopes. In addition, distributing workstations allows ensuring system functionality in case of one workstation damage. Furthermore, workstations could take the server's functionality to collect data. The system can be easily extended by sensor network in order to maintain the radio telescope by measuring vibrations, temperatures, motor speed and voltage, maximum and minimum turn positions, etc.

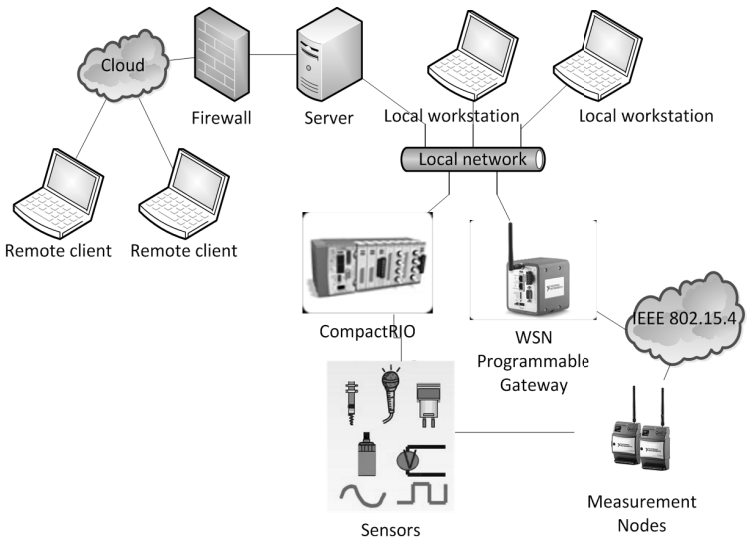

Fig. 3. *The proposed topological structure of the distributed real time data acquisition system*

The proposed flowchart of data acquisition is shown in Figure 4, which represents data collected only from one sensor. In order to implement the entire system with parallel sensing there also should be parallel loops. All data acquisitions work on loops. The flowchart can be divided into two main parts by data location. The first part is cRIO and WSN programmable gateway with its software and LabVIEW applications, while the second part is the server and workstations (it can be only one computer) with appropriate software and LabVIEW applications. Data exchange between these parts (between the server and workstations) is established using Ethernet.

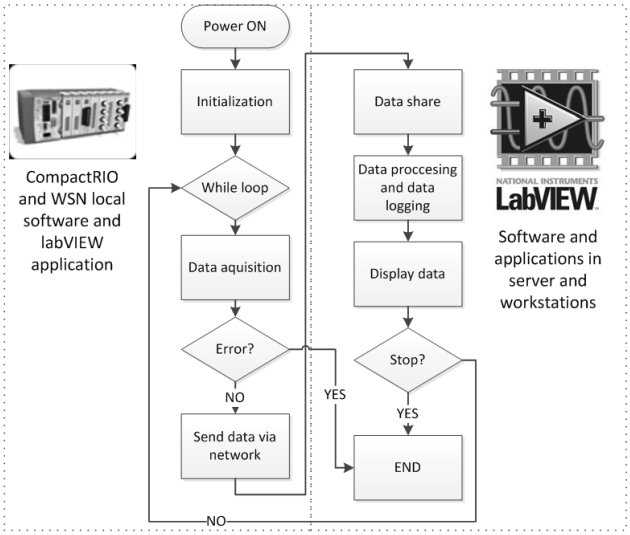

Fig. 4. *The flowchart of data acquisition system*

In order to test the system we developed model of the radio telescope based on National Instruments hardware and software. Design of DSC module application architecture is shown in Figure 5. Controller (DAQ) receives and translates inputs or requests data from the model. Controllers are responsible for implementation of the logic that updates the model based upon a set of rules and gets data from sensors. In some situations, the controller makes logical decisions about the input, before making a change to the model. The controller might send commands to the interface to make changes to it. Next, the interface obtains and presents data from the model.

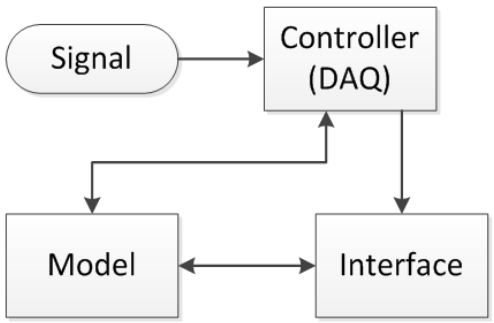

Fig. 5. *Design of DSC application architecture*

In addition, the interface renders the model as a form suitable for interaction and is fundamentally the user interface for the model. Next, the model represents the application state and main functionality associated with application data. These functionalities include logging, scaling, and alarming. The model must be independent, so it cannot refer to either the interface or controller portions of the application directly. The model passively supplies data to the other parts of the application.

4. Results

Radio telescopes located in Irbene (Latvia) are very important radio astronomy instruments for the Baltic Sea region. In order to develop an effective control system, it is required to get system characteristics by implementing data acquisition system, and as we found out early the best choice is the distributed data acquisition system. The control system and accurate monitoring system allow the radio telescope to produce larger amounts of very valuable and precise scientific space data.

We designed the prototype of distributed real-time data acquisition system using LabVIEW Datalogging and Supervisory Control (DSC) module capabilities (Figure 6), LAbVIEW software, NI CompactRIO Controller/Chassis with modules NI 9215, NI 9401, NI9421, wireless sensor network (WSN) programmable gateway NI 9792 and two nodes NI 3202. It has a sample rate up to 100 kS/s, 16-bit resolution and voltage range from -10V to 10V for analogue signals and clock rate up to 10 MHz, input range from 0V to 24V for digital signals. Moreover, the system's operating temperature range is from -40°C to 70°C. It is very important requirement of the system because hardware should be located in unheated areas of the radio telescope RT-16.

Designed distributed data acquisition system can visually represent data and save it for further research. Also, all parameters of vibrations, temperatures, motor speed and voltage can be accessible in a local network for other distributed applications. LabVIEW project was

tested in a laboratory using virtual signal generators and the results showed good visual capabilities. Furthermore, the analysis of hardware data sheets showed that such a system can reach high performance, with a potential measurement accuracy of analogue signal of 0.0015%. However, for real system monitoring further analysis of sensors considering measurement accuracy, signal filtering and data processing is needed.

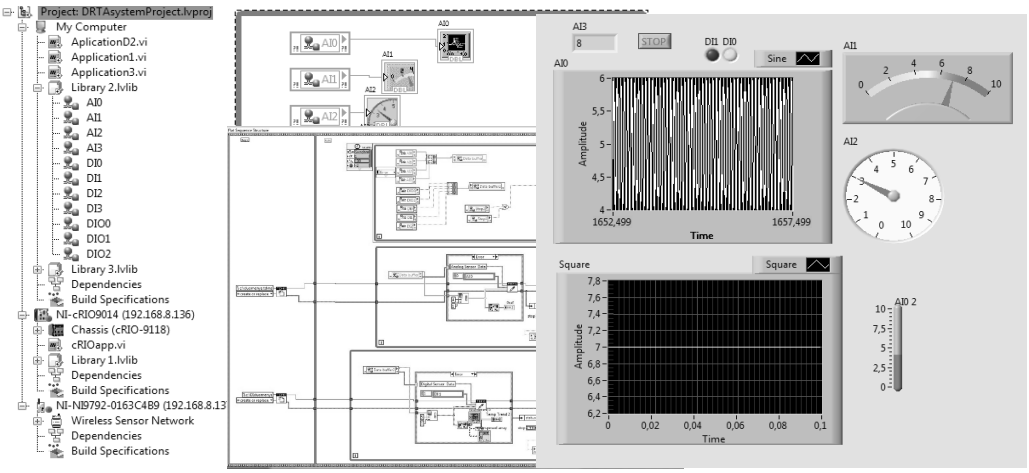

Fig. 6. *Designed LabVIEW project of distributed real time data acquisition system*

5. Conclusions

Analysis of literature and data sheets showed that distributed systems are more commonly used in the complicated systems. These systems have many advantages in comparison with centralized systems, such as increased reliability and accuracy, possibility of multiple devices in one system, and reduced costs associated with cabling and maintenance. The conceptual model of distributed radio telescope monitoring system was proposed and prototype of the system was designed using National Instruments hardware (cRIO controller, WSN) and LabVIEW software tools. The test results of the distributed real-time data acquisition system prototype showed very good visual capabilities and performance including sampling rate of 100 kS/s and measurement accuracy of 0.0015% could be achieved for analogue signals and clock rate up to 10 MHz for digital signals.

In the next step, a sensor network for radio telescope should be designed and acquisition of real measurements made.

6. Acknowledgements

The authors thank the Project LLIV-215 "JRTC Extension in Area of Development of Distributed Real-Time Signal Processing and Control Systems" for the possibility to complete a scientific research.

7. References

1. Sarfi, T., Semancik, J. (2007). Advantages of a Distributed Data Acquisition Approach. *2007 IEEE Autotestcon*, pp. 567-572.

2. Jiang, H., Kesteven, M., Wilson, W., Li, C.T., Hiroaki, N., Chen, M. T., Huang, T., Koch, P., Chang, J., Kubo, D. (2009) A Distributed Control System for a Radio Telescope with Six-Meter Hexapod Mount. *IEEE International Conference on Control and Automation*, pp. 2003-2010.

3. Berruti, L., Davoli, F., Zappatore, S. (2012). Performance evaluation of measurement data acquisition mechanisms in a distributed computing environment integrating remote laboratory instrumentation. *Future Generation Computer Systems*, 29 (2), pp. 460–471.

4. Ren-gui, L., Pei Lei, Ma Rui, Wei Jun-lei, Zhu Chun-bo (2009). EV Energy Storage Monitoring System Based on Distributed Data Acquisition. *2009 IEEE Vehicle Power and Propulsion Conference*, pp. 1386-1389.

5. Zhang, B., Zhang, L., Liu, K. (2011). Distributed Data Acquisition and Hierarchical Signal Process for Flight Simulator. *2011 Eighth International Conference on Fuzzy Systems and Knowledge Discovery FSKD*, pp. 2422-2426.

6. Na, L., Liangping, F., Bing, Z., Xiaofei, S., Zhu, L., Hao, X. (2010). A Study on a cRIO-based Monitoring and Safety Early Warning System for Large Bridge Structures. *2010 International Conference on Measuring Technology and Mechatronics Automation*, pp. 361-364.

7. Jun, L. (2009). High Performance Distributed Data Acquisition System for long-term Bridge Health Monitoring. *2009 International Conference on Computational Intelligence and Software Engineering*, pp. 1-3.

8. Qin, Z., Yu, G. (2012). Technique of Data Acquisition for Linear Induction Motor based on LabVIEW. *2012 International Symposium on Instrumentation & Measurement, Sensor Network and Automation IMSNA*, pp. 553-556.

9. Hua, Z. (2011). Application of LabVIEW in the Design of Data Acquisition and Signal Processing System of Mechanical Vibration. *2011 International Conference on Mechatronic Science, Electric Engineering and Computer*, pp. 2551-2554.

10. Wang, H., Li, D.D., Xue, P., Zhu, J., Li, H. (2012). LabVIEW-based data acquisition system design. 2012 *International Conference on Measurement, Information and Control MIC*, pp. 689-692.

11. Rodriguez, J., Tello, C. (2008). Intelligent Wireless System to Monitoring Mechanical Fault in Power Transmission Lines. *Electronics Robotics and Automotive Mechanics Conference CERMA 08*, pp. 99-104.

12. Guofang, L., Lidong, C., Yubin, Q., Shengtao L., Junyu, X. (2010). Remote Monitoring System of Greenhouse Environment Based on Lab VIEW. *International Conference On Computer Design And Appliations ICCDA 2010*, pp. V2-89-V2-92.